RSC Advances

ROYAL SOCIETY OF CHEMISTRY

www.rsc.org/advances

RSC Advances

RSCPublishing

ARTICLE

Fabrication of bioactive glasses-introduced nanofibrous membranes with multifunctions potentially for wound dressing

Cite this: DOI: 10.1039/x0xx00000x

Received 00th January 2012,
Accepted 00th January 2012

DOI: 10.1039/x0xx00000x

www.rsc.org/

Weibin Ma[a], Xianyan Yang[a], Liang Ma[a], Xingang Wang[b], Lei Zhang[c], Guojing Yang[c], Chunmao Han[b], Zhongru Gou*[a]

Currently, a variety of polymer-based membranes are available which differ in the compositions and microstructures, but far away from the treatment of chronic, nonhealing wounds. Herein we design a new bioactive glass (BG)-introduced multifunctional gelatin/chitosan (G/C) nanofibrous membranes for chronic wound healing, due to the efficacy of chitosan and BG for antibacterial and wound healing properties. Water contact angle of the mats increased and water uptake capacity decreased with increasing BG content, suggesting their surface hydrophilicity could be adjusted by BG component. The biologically active ions were readily released from the mats potentially favorable for infectious wound. Also, the G/C-BG mats were well tolerated by the surrounding host tissue without causing any inflammation, but were fully degraded in subcutaneous tissue in rats after 4 weeks postoperatively. Therefore, the G/C-BG mats could afford a close biomimicry to the fibrous nanostructure of natural soft tissues to facilitate chronic, nonhealing wound treatment.

1. Introduction

In wound operations, the purpose of dressing the wound is to promote an optimal healing environment by providing pain relief, protection from trauma and infection, a moist environment, and removal of debris. By simultaneously maximizing the patient's nutritional status and providing meticulous wound care, most wounds will heal appropriately[1]. However, the chronic, nonhealing wounds are involved progressively tissue loss and bacterial colonization, particularly in venous stasis, diabetic ulcer, and bed sores, and thus give rise to big challenge to wound-care product researchers[2,3,4].

It is known that calcium is an important factor in the wound healing of skin and assuming that it is required for the migration of epidermal cells[5]. Clinically, the direct topical application of calcium to chronic wounds through calcium alginate dressings has been shown to be beneficial[6]. On the other hand, bacterial invasion may make the wound unsuitable for skin regeneration due to the growth of bacterial population. So the goal of wound dressing is to produce an ideal structure with high porosity and antimicrobial activity which can also be a good barrier. Recently, some studies have found that the local release of the inorganic ions from bioactive glasses (BGs) can suppress microorganisms, stimulate collagen production, and accelerate wound healing process[7-10]. It was found out that BGs can be combined with the soft tissue and promote soft tissue regeneration[11]. Moreover, BG can also reduce the inflammatory response and wound exudate, and has certain antibacterial and hemostatic potential, which have a positive therapeutic effect on the wound[12]. Wilson et al. firstly showed that soft connective tissues could form a bond to 45S5 Bioglass® and established the safety use of particulate forms in soft tissue if the interface was immobile[13]. More recent studies demonstrated the beneficial effects of 45S5 Bioglass® and borate-containing 13–93 BGs to promote angiogenesis, which is critical to the healing of soft tissue wounds[14,15]. Thus, the development of BG-loaded porous wound dressings with antimicrobial activity is highly desired.

Electrospinning is a versatile technique for bridging the gap between natural extracellular matrix (ECM) and artificial materials. With its simple manufacturing equipment, low cost, and controllable process, electrospinning has become one of the main approaches to prepare nanofibrous materials. It offers a range of benefits, including the ability to produce continuous nanofibers, controllable ECM-mimicing nanostructures and thus enhance the cell migration and proliferation[16]. Wound dressings via electrospinning can meet the requirements such as higher gas permeation and protection of wound from infection and dehydration, for electrospinning materials have higher porosity and huge surface area[17]. It is also important to select the appropriate materials to guarantee the biocompatibility and biodegradability of the wound dressings. Gelatin has excellent biocompatibility and cell adhesion ability, is widely used in

clinics for wound dressings, pharmaceuticals and adhesives owing to its biodegradability and hydrogel characteristics, as well as its formability and cost efficiency[18]. However, gelatin, as a kind of hydrolysis derivative of collagen, possesses quite a number of ionizable groups, and additionally, the strong hydrogen bonding results in a three-dimensional (3D) macro-molecular network, which makes the mobility of the gelatin chains decrease tremendously and poor electrospinnability[19,20]. Chitosan is a natural positively charged basic polysaccharide and has been shown to exhibit some pharmacological activities including antimicrobial, anti-inflammatory, anti-adhesion, and wound healing effects[21]. Javad et al. has prepared gelatin/chitosan (G/C) nanofibers using acetic acid solution[22]. However, it is still a great challenge to treat the chronic, nonhealing wounds with these pure polymeric materials[2,23].

Most recently, we developed a nanofibrous gelatin (NF-GEL)/BG composite hydrogel by phase separation method and followed by arming the nanofibers network with counterionic chitosan-hyaluronic acid pairs for improving microstructural and thermal integrity[24]. This NF-GEL-based hydrogel could afford a close biomimicry to the fibrous nanostructure of the natural soft tissues, but its overhigh water uptake capacity (~900%) is potentially disadvantageous for accumulation of fluid in the moist wound areas. In this regard, herein we designed a new G/C-based nanofibrous membrane as wound dressing with high biocompatible and bioactive properties (see Scheme 1). We explored the fabrication of G/C membranes in the presence of BG superfine particles. The BG with the composition of SiO_2-CaO-B_2O_3-P_2O_5-CuO-ZnO-K_2O-Na_2O was chosen based on their specific biological performances in wound healing process. Calcium, potassium, and sodium are well known to be essential for promoting epithelial repair during wound healing process. Moreover, both of copper and zinc are suggested to have the ability of promoting skin regeneration and antimicrobial activity in wound healing process[25,26]. Boron may modulate the turnover of the extracellular matrix and enhance the collagenase and cathepsin D activities in fibroblasts[27]. To our knowledge, this study is the first time to investigate the electrospinnability of the multi-component BG-introduced G/C aqueous solution for wound dressings, and then its physicochemical properties and biocompatibility were studied potentially for treatment of chronic wound healing.

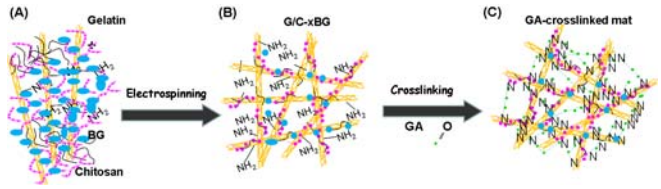

Scheme 1. Schematic illustration of the preparation procedure of the BG-introduced G/C nanofibrous membranes.

2. Materials and Methods

2.1 Materials and chemicals

Chitosan (MW, 50 kDa) with a degree of deacetylation of 90% was purchased from Haidebei Marine Bioengineering Inc, China. Gelatin (type B, from bovine), tetraethyl orthosilicate (TEOS; 99.99%), triethyl phosphite ($P(OEt)_3$; 99.50%), and the inorganic salts were purchased from Sinopharm Chemical Reagent Co., China. All the chemicals were of analytical grade and were used directly without further purification.

2.2 Synthesis of BGs

The BGs with 30.0 SiO_2, 27.0 CaO, 20.0 B_2O_3, 4.0 P_2O_5, 1.5 CuO, 1.0 ZnO, 3.0 K_2O, and 9.0 Na_2O (wt%) was prepared by a sol-gel process according to our previous work[28]. In brief, HCl, H_3BO_3, TEOS, and $P(OEt)_3$ were added into ethanol-water mixture and stirred for 20 min. The nitrates of calcium, sodium, copper, zinc, and potassium were then added into deionized water (Di water) under magnetic stirring for 20 min. The solutions were mixed and subsequently, aged at 80°C for 36 h and calcined at 680°C for 90 min. The as-obtained BG powders were ball milled for 4 h to reach a smaller particle size and characterized by scanning electron microscopy (SEM; JEM-6700F). The particle size distribution data were collected by DLS in a Mastersizer 2000 analyzer (Malvern Instuments Ltd.).

2.3 Electrospinning of G/C-xBG membranes

Gelatin was dissolved in Diwater to form the concentration of 25 wt% and chitosan was dissolved in acetic acid solution (70 wt%) to form the concentration of 3.0 wt%. Then, the gelatin solution, chitosan solution and BG powders were mixed with different ratios under magnetic stirring to form organic-inorganic hybrid suspension (Table 1).

Table 1. Composition in electrospinning solutions.

Samples	Gelatin (g ml^{-1})	Chitosan (g ml^{-1})	C/G (*m*/*m*)	BG/(G+C) (*m*%)
G/C19	17.23	0.91	1/19	0
G/C17	9.94	1.75	3/17	0
G/C15	6.64	2.16	5/15	0
G/C-0BG	9.94	1.75	3/17	0
G/C-6BG	9.94	1.75	3/17	6
G/C-12BG	9.94	1.75	3/17	12
C/C-15BG	9.94	1.75	3/17	15

The suspension solutions with chitosan/gelatin (C/G) ratio of 1:19, 3:17 and 5:15 in the presence and absence of BGs were poured into a 15 ml plastic syringe equipped with a 20-gauge metal needle, which was then placed on the infusion syringe pump to modulate the pump rate at 0.2 ml h^{-1}. The needle was connected to a high-voltage generator (0–50 kV; Dongwen High Voltage Inc., China). The device was placed in a chamber that provided flowing warm air. A 13 kV voltage was used, and the grounded Al collector was placed at 12 cm from the needle tip. The fibers were electrospun onto the collector and formed G/C-*x*BG [*x*=0, 6, 12, 15%; *x* is denoted as BG/(G+C) percent ratio in the electrospinning solutions] fibrous membranes.

2.4 Chemical cross-linking of the G/C-*x*BG membranes

After the electrospun membrane was dried in vacuum for 24 h, glutaraldehyde (GA) vapour cross-linking was carried out by placing the membrane above GA solution (25 wt %) in a sealed dessicator at room temperature for 48 h[29]. Then the GA-cross-linked G/C-*x*BG membranes were washed three times with distilled water and followed by drying in vacuum. The microstructures of the G/C-*x*BG membranes were characterized by SEM and energy dispersive spectrometer (EDS). The thermal analysis of the membrane samples was carried out with the heating rate of 10°C min^{-1} from 20°C to 900°C in air, using a thermogravimetric and differential thermalgravimetric analysis (TG-DTA; Perkin Elmer, USA). FTIR spectra of samples were obtained using Fourier transform infrared spectroscopy (Nicolet). The spectra were collected over the wave number range of 400–4000 cm^{-1}.

2.5 Mechanical characterization

The mechanical properties of the samples were characterized using a multipurpose tensile tester (KES-GI; Kato-Tech, Japan) in tensile mode[30]. Firstly, a white paper was cut into a template with width × gauge length, and double-side tapes were glued onto the top and bottom areas of one side. The mats with a planar dimension of 5 mm×40 mm were then glued onto the top and bottom sides of the paper template along the vertical lines. Each sample was firstly stored under 65% relative humidity at 20°C for 24 h and then tested at 2 mm min^{-1} elongation speed for four times.

2.6 Water contact angle (WCA) measurement

The static WCA of the G/C-*x*BG membrane was measured by using a DSA100 drop shape analysis system (Krüss, Germany), an image was taken with the built-in digital camera. The average static WCA was obtained from three points of each sample and 3 μl deionized water was used in each experiment (23°C).

2.7 Equilibrium water uptake capacity (WUC) and area change ratio (ACR) measurement

The swelling ratio was determined by immersing the porous membranes in MiniQ water at 37°C for 4 h and was considered to reach the equilibrium of water uptake. The WUC and ACR were quantified as: WUC (wt%)=(W-W0)/W0×100 and ACR (S%)=S_s/S_d×100, where W0, W are the dry weight and wet weight of the samples before and after immersing in water and removing the surface water with filter paper; S_d, S_s are the original area of membranes and the measured area of swelled membranes after immersing in water, respectively.

2.8 Inorganic ion release test in vitro

The inorganic ion release was investigated for the G/C-*x*BG membranes (5 cm× 5 cm; ~150 μm in thickness) by immersing in 5 mL Tris buffer (0.02 M) with an initial pH 7.20 at physiological temperature in vitro. After immersing for different time intervals, changes in pH of aqueous medium were measured firstly; then 0.5 ml of supernatant was diluted in 5% HCl solution, and aliquot amount of fresh buffer (0.5 ml) was added into the buffers to maintain the solution volume constant. The inorganic mineral elements including calcium (Ca), zinc (Zn), copper (Cu), boron (B), and silicon (Si) in the supernatant were determined using inductively coupled plasma spectrometry (ICP; IRIS INTREPID II XSP, Thermo) analysis.

2.9 In vitro antibacterial test

Direct antimicrobial activity of the BG disks (Ø 6 mm×2 mm) was tested by agar diffusion using actinomyces viscosus (*A.viscosus*) and Escherichia coli (*E. Coli*). The disks were prepared in stainless steel mould and sintered at 650°C for 90 min. The sintered disks of commercially available 45S5 Bioglass® (US Biomaterials Co.) was used as control. The disks were allowed to set at 37°C and 100% humidity for 24 h. The bacterial strains were maintained as subcultures on trypticase soy agar (TSA) plates at 37°C in an anaerobic chamber, where O_2 and H_2 were purged down to 100 ppm and 1%, respectively, using N_2 and biological atmosphere mixture (5% CO_2 in N_2). The BG disks were placed at the centre of the agar plate and the inhibition zone around the disks were observed using SEM observation after incubation for 16 h.

2.10 In vivo biocompatibility test

The procedures for the use of animals were in accordance with the animal care and use committee of Zhejiang University. Prior to implantation, the membranes were UV light sterilized from different directions, each side 45 min. Adult Sprague Dawley (SD) rats weighing 250–380 g were anaesthetized with 0.25 ml IM Hypnorm (0.315 mg ml^{-1} fentanyl citrate and 10 mg ml^{-1} fluanisone) and 1 mg IP diazepam. A midline incision of 2–3 cm was made through the shaved skin on the backs[31]. The G/C-0BG and G/C-15BG membranes were then implanted into the subcutaneous pockets on the right and left hand side of the incision. After 1, 2 and 4 weeks of implantation, the rats were sacrificed using pentobarbitone (200 mg ml^{-1}), and optical images of the membranes and subcutaneous tissues were taken.

2.11 Statistical analysis

The results were expressed as mean ± standard deviation (mean ± SD). Statistical significance was tested by one-way ANOVA test, and differences of $p<0.05$ were considered to be statistically significant.

3. Results and discussion

3.1 Morphology characterization

It is known that the pure gelatin solution is usually in a hydrosol state at above physiological temperature, and when gelatin concentration is high enough and its temperature is decreased to below 37°C, the hydrosol transform into hydrogel. Thus introduction of another polymer component (e.g. chitosan) into gelatin matrice is of high significance because the pure gelatin fibers are very brittle and unstable in aqueous environment. Figure 1 shows the SEM images of the electrospun G/C mats with different C/G weight ratio (1/19,

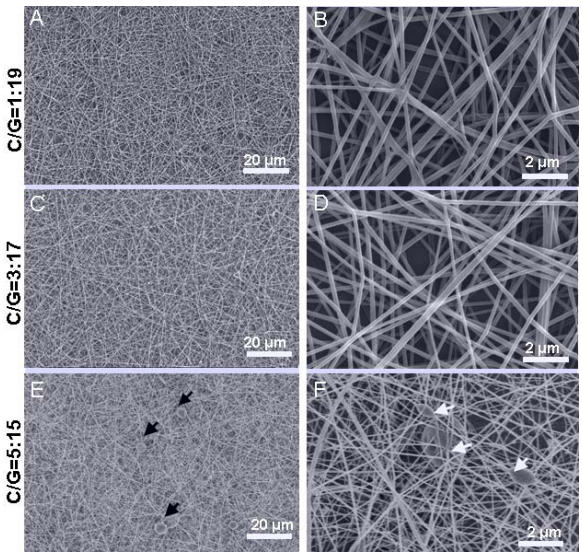

Figure 1. SEM images of the G/C nanofibrous mats with different C/G mass ratio.

3/17, 5/15). It was evident that the G/C membranes were composed of open pores with several microns in size, and the pore wall was made of thin fibers. With increasing C/G ratio from 1/19 to 5/15 in the solutions, the beads could be seen in the fiber body, and was prone to aggregation. It should be mentioned that the parameters, such as electric field and spinning distance, were examined for studying the effects of C/G ratio in the solutions (i.e. 3/17, 5/15, 6/14) on electrospinnability and morphology of gelatin at the concentration of 17.23 g ml^{-1}. It was found that gelatin nanofibres were hardly obtained until the gelatin concentration reduced to 9.94 and 6.64 g ml^{-1} and weight ratio of chitosan and gelatin increased to 3/17 and 5/15. Furthermore, when the weight ratio of chitosan and gelatin exceeded 6/14, it was not almost possible to get well shaped fibres (Not shown). These primary results suggested that the electrospinning of G/C composite fibers mainly work at C/G ratio between 1/19 and 3/17. In order to endow the multifunctions of the composite membranes, the electrospun G/C-based fibrous membranes with C/G/ ratio of 3/17 and appropriate amount of BG addition is highly interesting in both fundamental and practical aspects.

Sol-gel method is versatile to prepare nanoscale BG powders in comparison to the high-temperature calcination treatment. The measured composition of powders were 30.4 SiO_2, 27.2 CaO, 19.6 B_2O_3, 3.7 P_2O_5, 1.6 CuO, 1.1 ZnO, 3.2 K_2O, and 8.7 Na_2O (wt%), similar to the theoretical values as mentioned above. SEM observation in Figure 2A shows that the sol-gel-derived BGs were highly dispersible with nanoscale dimension in particle size. Meanwhile, the quantitative analysis confirmed that the BG powders had very narrow particle size distribution in 840–1660 nm (Fig. 2B), suggesting such BG is favorable for electrospinning with organic component.

According to the SEM observation (Fig. 3A-H), the G/C-*x*BG membranes with introducing different amount of BG at C/G ratio 3/17 via electrospinning technique showed some difference in the fiber morphology with increasing BG/(G+C)

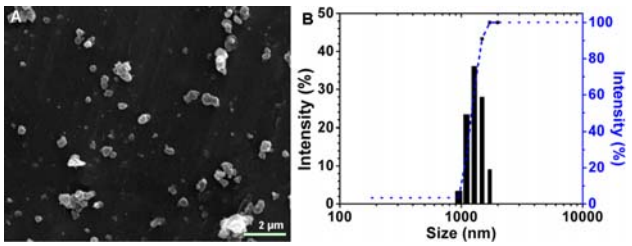

Figure 2. SEM observation (A) and particle size distribution (B) of BG powders.

ratio from 6% to 15%, but the fiber diameter ranged from tens to hundreds of nanometers, which was the same range as that of natural collagen matrices. The mats grew some blade-like continuous fibrous network with the BG/(G+C) increasing up to 12–15%, and the BG particles were anchored in the fiber matrix and scarcely naked in the porous network with increasing BG content. It is also noted from the EDX analysis (Fig. 3I–L) that the Si could be detected in the BG-introduced membranes, and the intensity of the silicon peak increases with the increase of BG content in the membranes. It should be mentioned that the BGs with appropriate inorganic oxide compositions are highly beneficial for antibacteria and soft regeneration in chronic wound[7-10]. Unfortunately, the mixture solution is poorly electrospun with increasing BG/(G+C) ratio up to 18%. Accordingly, these results suggest that the appropriate amount of BGs (i.e. 15%) could be successfully nested in the G/C nanofiber body.

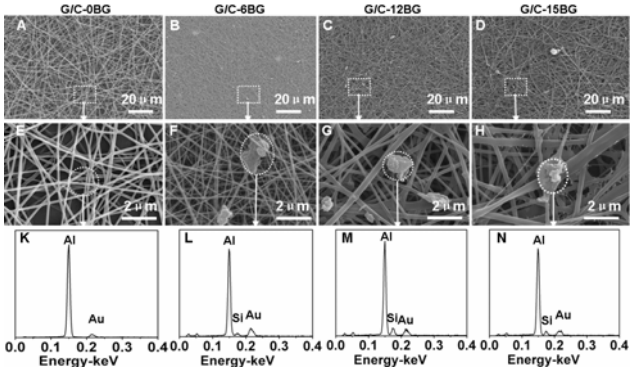

Figure 3. SEM observation (A–H) and EDX analysis (K–N) of the G/C-xBG membranes with introducing different amount of BG at C/G ratio 3/17 via electrospinning technique.

3.2 FTIR analysis

The G/C-*x*BG membranes and BG powders were characterized by FTIR to investigate the molecular changes after adding BG into the G/C nanofibrous mats. As illustrated in Figure 4A, the FTIR spectra of all membrane samples had the similar roughness. Amide I (~1650 cm^{-1}) and amide II (~1550 cm^{-1}), which are common bands of protein and corresponding to the stretching vibrations of C=O bond and coupling of bending of N–H bond and stretching of C–N bonds[32], were attributable to gelatin which is a derived from collagen by controllable hydrolysis. Other distinct bands such as C=C (~1410 cm^{-1}) and C–O (~1038, 1241, 1080 cm^{-1}) were contributed to gelatin and

chitosan. The FTIR spectra of BG reveal the bands at Si-O-Si bend and P-O stretch at 462 cm^{-1} and 1037 cm^{-1}, respectively[33]. From Figure 4B, the FTIR spectra of BG, G/C-0BG and G/C-15BG were put together to show the difference. In particular, from Figure 4C which is a magnified spectrum from 400−550 cm^{-1}, Si–O–Si bend peak is shown on the spectra of BG and G/C-15BG, but not on the G/C-0BG which is made up of pure polymers. These results suggest the superfine BG particles are readily introduced into the electrospun G/C composite fibers.

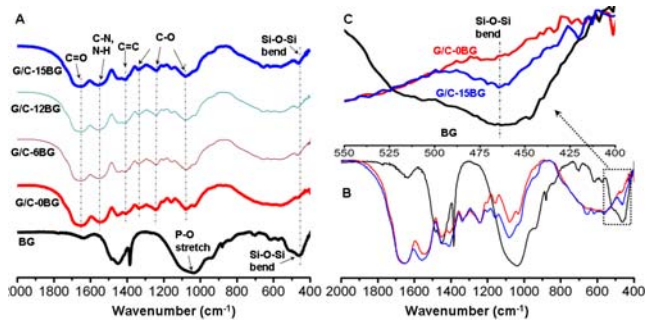

Figure 4. FTIR spectra (A) of G/C-*x*BG nanofiberous mats. (B, C) The magnified FTIR spectra.

3.3 TG-DTA analysis

The G/C-*x*BG mats and BG powders were further analyzed by TG-DTA (Fig. 5). From the DTA curve of BG, no strong exothermic or endothermic behavior was seen. And the total weight loss of BG was about 22% mainly due to the removal of the adsorbed moisture and the pyrolysis or decomposition of residual nitrate groups and organic components in the sol-gel synthesis process[34]. As for the G/C-*x*BG membranes, there was an endothermic event in 35–150°C with weight decrease by 13% due to the loss of adsorbed water. The significant weight loss (up to 76~83%) is recorded in the temperature range of 200–530°C, and this is accompanied by a strong exothermic peak at 450–530°C which is caused by the pyrolysis of gelatin and chitosan components. Evidently, the mass residual of the G/C-6BG, G/C-12BG and G/C-15BG mats were consistent with the introduced mass percent of the BG in the precursor solutions, by increasing the amount of BG in the G/C mixture solutions, the strong exothermic peak has a tendency to be at a lower temperature and the remains tends to increase after the entire thermal weight loss process, compared to the G/C-0BG

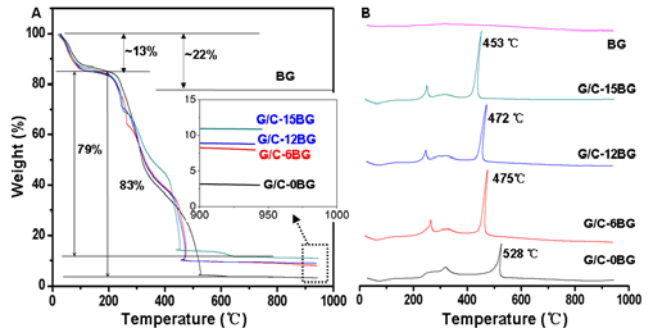

Figure 5. TG (A) and DTA (B) curves of G/C-xBG nanofibrous mats and pure BG.

3.4 Mechanical analysis

Tensile strength was measured to confirm the operability of the mats. Figure 6 shows the representative stress-strain curves, and Table 2 shows the mechanical data and elongation at break. It can be seen that the BG-introduced mats exhibited considerable tensile strength (up to two to fourfold higher than that of pure organic mats), meanwhile the increase of BG content produced a further increase in mechanical strength, indicating that the inorganic-organic interaction between G/C and BG could reinforce the mechanical stability of the mats. More precisely, the average elongation ratio of the mats increased by nearly 150% after 15% BG addition, thus making it considerably favourable for biomedical applications.

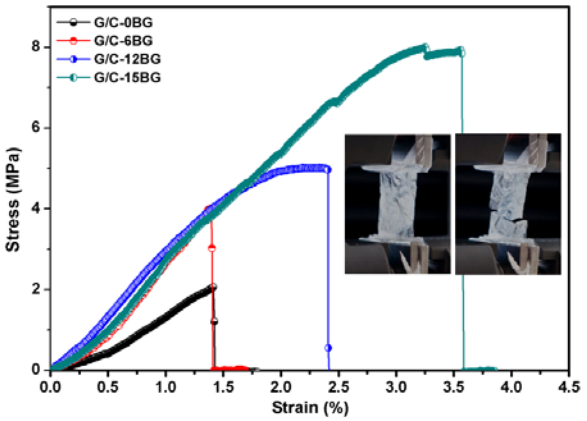

Figure 6. Representative stress-strain curves of the G/C-*x*BG nanofiberous mats (Insets showing the optical images of the mats before and after mechanical test).

Table 2. Mechanical data of the electrospun mats.

Samples	Tensile strength (MPa)	Young's modulus (MPa)	Elongation at break (%)
G/C-0BG	2.05	132	1.41
G/C-6BG	4.00	268	1.39
G/C-12BG	5.00	244	2.39
C/C-15BG	7.92	269	3.56

3.5 WCA analysis

It is well agreed that hydrophilicity influences the adsorption of blood proteins, and especially the cell attachment behavior may be regulated through these proteins[35]. Samples which produce small contact angles with blood are, in general, associated with good blood compatibility, whereas those with large contact angles have relatively high anti-adhesion ability[36]. Thus, the surface-responsive behavior of the electrospun mats with different BG contents was analyzed by measuring the static WCA (Figure 7). The pure organic G/C-0BG mats were quite hydrophilic, presenting an average contact angle of 20.4°. In contrast, the hydrophobicity of organic-inorganic hybrid mats was substantially created by BG/(G+C) percent ratio in the mats. Contact angle was slightly increased to 47.4° after introducing 6% BG, and significantly increased up to 84.9° and 94.6° with adding 12% and 15% BG, which was related to the role of microscopic BG particles embedded in the nanofibers.

This is consistent with the fact that WCA measurements are significantly affected by several parameters, namely topographical roughness and composition. By looking at the SEM images in Figure 3, it is evident that the roughnesses of G/C-*x*BG without and with introducing BG are different, at least at the submicron length scale. In fact, the hydrophilic-to-hydrophobic transition phenomenon for the hybrid mats is attributed to relatively rougher surface, and in particular responsive wettability change is greatly amplified on rough substrates with micro- and nanostructures, and increases significantly with the increase in roughness[37,38]. This means that the hydrophilicity of the electrospun mats can be adjusted by changing the amount of BGs.

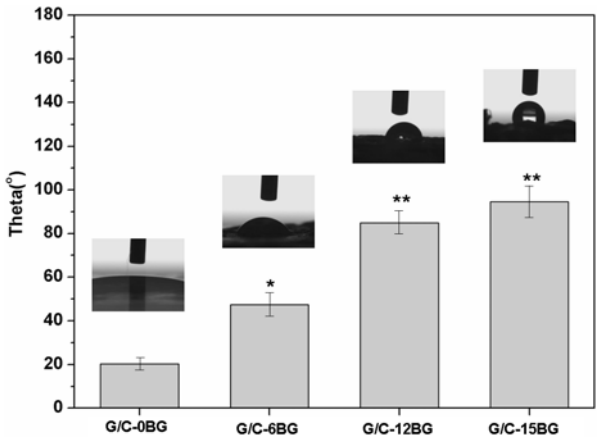

Figure 7. Water contact angles (WCA) of the G/C-*x*BG nanofibrous mats (* $p<0.05$ significantly different from G/C-0BG; ** $p<0.01$ significantly different from G/C-0BG).

3.6 WUC and ACR analysis

It is known that the wound areas should be kept just moist enough to obtain the benefits of accelerated healing; but there should be no accumulation of fluid between the wound and the dressing to avoid infection. Figure 8 shows the WUC and ACR which had opposite trends with increasing BG content. The polymer membrane free of BG after cross-linking treatment had the highest (721.15±21.30%), its ACR was 98.28±0.75 v/v%. By contrast, the WUC of the sample with highest BG/(G+C) ratio (15%) reduced to 217.8±10.8% but its ACR changed few (99.64±0.47%). These results suggest that the cross-linked G/C-*x*BG become more rigid and the incorporation of BG in the polymer matrix readily reduce its water uptake capacity.

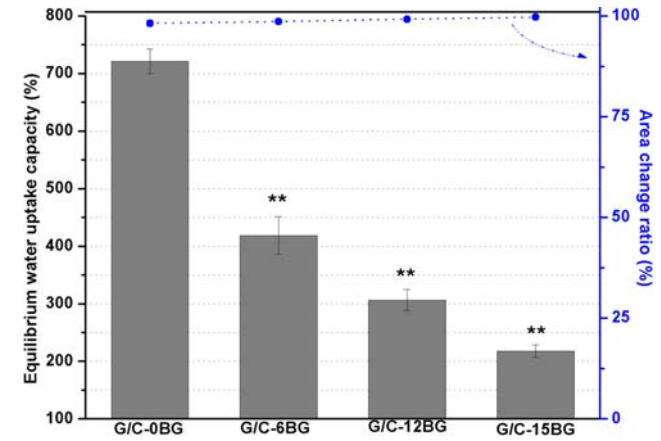

Figure 8. Water uptake capacity and area change ratio of the G/C-*x*BG nanofibrous mats (** $p<0.01$ significantly different from G/C-0BG).

3.7 Inorganic ion release analysis

To distinguish the contribution of BGs for the inorganic ion release, different immersion times, the G/C-*x*BG mats with different BG contents were investigated (Fig. 9A-E). As for the G/C-15BG sample, the rapid calcium and boron accumulation took place in the aqueous media within the initial 4 h, accompanying with a steady release of silicon, zinc and copper. Also, the copper and zinc concentrations were over 2.0 ppm and 0.8 ppm after immersion for 24 h, indicating the antibacterial inorganic ion dose in the immersion media can be accelerated with prolonging immersion time. In contrast, the inorganic ions were hardly measured in the medium during soaking the G/C-0BG mat. Indeed, the overall concentrations of calcium ions for the G/C-15BG increased markedly from the initial zero to nearly two-fold of calcium ions for the G/C-6BG sample in the media within 8 h, and thereafter both kept stable without much fluctuation (Not shown).

It is seen that the pH value in the medium immersing G/C-15BG showed a rapid increased from the initial value of 7.2 up to 8.6 within 8 h (Fig. 9F), and the greatest rate of pH increase was recorded within the first 4 h, and within 24 h the plateau (pH ~9.0) was reached, which would be effective in inhibiting

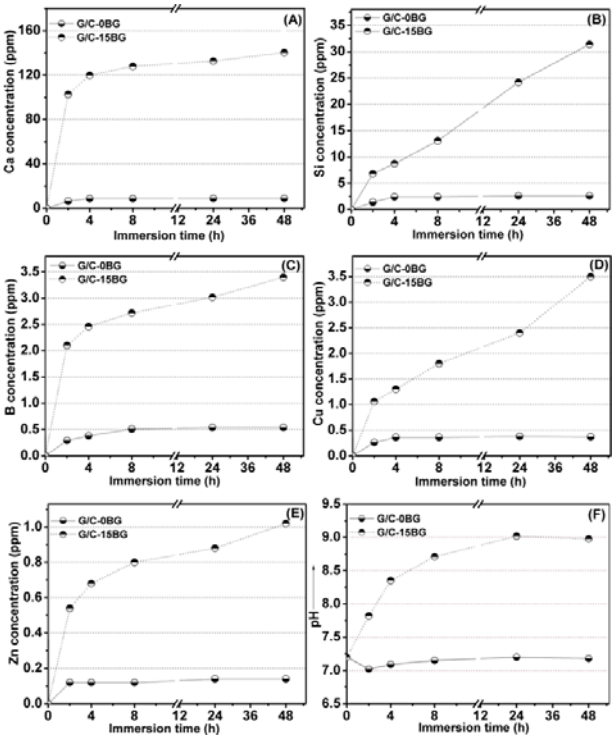

Figure 9. Ion release from the PBS medium (A-E) and changes in pH (F) when immersing the G/C-0BG and G/C-15BG mats, respectively.

the growth of some bacteria[8,9]. However, the pH value in the Tris buffer immersing the pure polymer mats showed a slight decrease (~7.05) within the initial two hours and then slightly increased up to nearly 7.2. This is possibly attributed to the acetic acid residual which has been used to dissolve chitosan. Moreover, it is stressed that the ion concentration values varied depending on the BG content, similar trends in pH change were observed for all of G/C-*x*Cu mats (Not shown).

3.8 In vitro antibacterial evaluation

The BG formulations inhibited growth of *A. Viscosus* and *E. Coli*, as clear rings appeared around disk samples inserted into the agar plate. The BG markedly inhibited the growth of *A. viscosus*, producing a larger zone of inhibition than that for 45S5 Bioglass® (Fig. 10A). Meanwhile, the 45S5 Bioglass® appeared to cause much lower inhibition effect on *E. Coli* than the BG containing CuO and ZnO; for instance, the 45S5 Bioglass® had no substantial effect on the bacterial viability of *E. Coli* (Fig. 10B), similar to the results reported previously[39]. These results also demonstrate that an appropriate level of ZnO and CuO introduction in BG have a considerable effect on inhibiting the microbial viability.

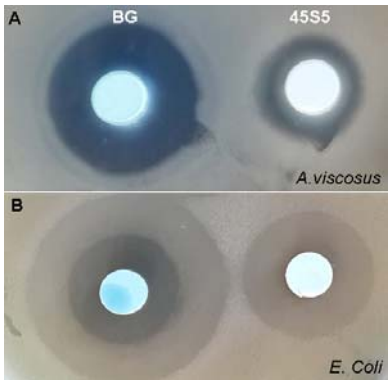

Figure 10. Agar diffusion test of the BG and 45S5 Bioglass® formulation with *A.viscosus* (A) and *E. Coli* (B) bacterial stains.

3.9 In vivo biocompatibility evaluation

Gelatin is available via a controlled hydrolysis of collagens, which is one of the most abundant structural fibrous insoluble proteins throughout body. The gelation temperature of GEL is very close to the human physiological temperature, and accordingly the gelatin-based dressings must be crosslinked to improve its thermal and structural stabilities in the wet state. As shown in Figure 11, both of GA-crosslinked G/C-0BG and G/C-15BG mats were well tolerated by the surrounding host tissue without causing any inflammation in rat subcutaneous tissue after one and two weeks of implantation, which indicates the mats is highly biocompatible. Interestingly, the G/C-0BG and G/C-15BG mats were degraded in subcutaneous tissue after 4 weeks of implantation, implying the mats are of good biodegradability. It is reasonable to postulate that the G/C-6BG and G/C-12BG mats have the similar performances. The characterization of biocompatibility and biodegradability of nanofibrous mats are perfectly match the needs of wound dressing. Evidently, the excellent biocompatibility of the mats is due to the intrinsic quality of the ingredients and the nanofibrous structure.

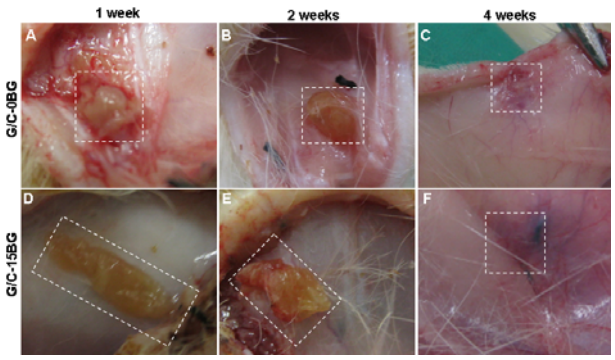

Figure 11. Optical pictures of implanted G/C-*x*BG mats in the subcutaneous tissue in rat model.

It is known that biomimetic processes and especially high voltage electrospinning is well suited to generate nanofibrous porous membrane matrices directly from polymer solutions. Until now, many researchers have examined gelatin, chitosan, and BG, respectively, as promising materials for the acceleration of wound healing. Unfortunately, gelatin exhibits poor mechanical stability that is too brittle when fully dried or too soft when fully wet and is easily soluble in aqueous medium. On the other hand, chitosan is obtained by the hydrolysis of chitin and is the only cationic polysaccharide in nature, with outstanding wound healing effect[40]. Therefore, the primary objective of this study is to develop a G/C-based electrospun membrane dressing with improved biologically active and antibacterial properties. The ionic form of silver (Ag^+) is a well-known highly antibacterial material, and the silver-loaded dressing is also an increasingly popular approach in the control of wound bioburden[41]. However, a high concentration of silver impairs the functioning of the central and peripheral nervous systems[42,43]. In contrast, a variety of studies have demonstrated the angiogenic effects of BG, i.e., increased secretion of vascular endothelial growth factors (VEGFs) and VEGF gene expression in fibroblasts, the proliferation of endothelial cells and formation of endothelial tubules in vitro, as well as enhancement of vascularisation and wound healing in vivo[44, 45]. Furthermore, BGs may inhibit the growth of a wide selection of aerobic and anaerobic bacterial species typically causing infections on the surface of prostheses, and the antibacterial activity of BG correlated mainly with the ion doping, particle size, pH and high silicon ion levels in the supernatant[9,46]. Moreover, the ion products (e.g., Ca^{2+}, Na^+, K^+) dissolution from BGs have been demonstrated to be favorable for improving the electrospinnability of chitosan in our previous studies[47]. Therefore, the introduction of BG into the G/C composite membranes is highly desirable and beneficial for improving the chronic, nonhealing wound treatment.

It is assumed that the bioactive potential of G/C-xBG membranes can be attributed in two aspects: the inorganic ions

products from BG dissolution and the beneficial functions of G/C on the wound surface. These two constituents may be advantageous to mediating their activity in cellular signaling. Meanwhile, the BGs in the nanofibrous network provide a high antibacterial activity and modified surface properties, which would be helpful for anti-adhesion in wet wound areas. Therefore, it is postulated the BG-introduction endow improved biological performances for chronic wound healing. These results further support the hypothesis that the nanofibrous membranes have potential ability to enhance wound healing in pathological animal models. These studies will be presented in the near future.

4. Conclusion

In summary, the G/C-*x*BG nanofibrous composite membranes were successfully prepared using chitosan and gelatin dissolved with acetic and water, respectively. Then BG particles could be nested in the nanofibers and readily adjust the hydrophilicity of electrospun mats. The inorganic ion release from BG dissolution endows bioactive and antibacterial properties of the materials. The whole manufacturing process does not involve environmentally/biologically harmful additives and the mat products exhibit excellent biocompatibility, without involving any inert constituents. Therefore, this composition–structure relationship makes G/C-*x*BG nanofibrous mats more attractive candidates for potential uses as wound-healing accelerator in many chronic, nonhealing skin wound areas.

Acknowledgments

This work is supported by the National Science Foundation of China (51102211, 81301326, 81271956), the Zhejiang Provincial Natural Science Foundation of China (LZ14E020001, LQ14H060003), the Fundamental Research Funds for the Central University (2012QN81001), Research Fund of Zhejiang Provincial Education Department (Y201016210), and Shaoxing Science and Technology Bureau Foundation (2012B70016).

Notes

[a] Zhejiang-California International Nanosystems Institute, Zhejiang University, Hangzhou 310058, China. zhrgou@zju.edu.cn (Dr Z. Gou); Tel. +86 571-8820 8353.

[b] Department of Burns, The 2nd Affiliated Hospital, College of Medicine of Zhejiang University, Hangzhou 310009, China.

[c] Rui'an People's Hospital & the 3rd Affiliated Hospital to Wenzhou Medical University, Rui'an 325200, China

References

1 G.C. Gurtner, S. Werner, Y. Barrandon and M.T. Longaker, *Nature,* 2008, **453**, 314-321.

2 M. Ehrenreich and Z. Ruszczak, *Tissue Eng,* 2006, **12**, 2407-2424.

3 R. Word, *Surg Clin North Am,* 2010, **90**, 1195-1214.

4 M. Biswas, O. Gibby, T. Ivanova-Stoilova and K. Harding, *Int Wound J,* 2011, **8**, 99-102.

5 A.B.G. Lansdown, *Wound Repair Regeneration,* 2002, **10**, 271-285.

6 G.J. Motta, *Ostom Wound Management,* 1989, **25**, 52-56.

7 L.L. Hench, *J Mater Sci, Mater Med,* 2006, **17**, 967-972.

8 C.H.G. Martins, T.C. Carvalho, M.G.M. Souza, M.G. Souza, C. Ravagnani, O. E.D. Peitl, Zanotto, H. Panzeri and L.A. Casemiro, *J Mater Sci: Mater Med,* 2011, **22**, 1439-1446.

9 D. Zhang, O. Lepparanta, E. Munuka and H. Ylanen, *J Biomed Mater. Res*, 2009, **93A**, 475-483.

10 P. Wray, *Am Ceram Soc Bull,* 2010, **90**, 25-29.

11 T.B. Lovelace, J.T. Mellonig, R.M. Mefert, A.A. Jones, P.V. Nummikoski, and D.L. Cochran, *J Periodont,* 1998, **69**. 1027-1035.

12 J.J. Blakera, S.N. Nazhatb and A.R. Boccaccinia, *Biomaterials,* 2004, **25**, 1319-1329.

13 J. Wilson, G.H. Pigott, F.J. Schoen and L.L. Hench, *J Biomed Maters Res,* 1981, **15**, 805-815.

14 A.A. Gorustovich, C. Perio, J.A. Roether and A.R. Boccaccini, *Tissue Eng. B-Review,* 2010, **16**, 199-210.

15 M.N. Rahaman, D.E. Day, B.S. Bal, Q. Fu, S.B. Jung, L.F. Bonewald and A.P. Tomsia, *Acta Bioamterialia,* 2011, **7**, 2355-2364.

16 H. Li, Y. Xu, H. Xu and J.Chang, *J Mater Chem B*, 2014, **2**, 5492-5510.

17 K. A. Rieger, N. P. Birch and J. D. Schiffman, *J Mater Chem B*, 2013, **1**, 4531-4541.

18 C.S. Ki, D.H. Baek, K.D. Gang, K.H. Lee, I.C. Um and Y.H. Park, *Polymer,* 2005, **46**, 5094-5102.

19 Z. Huang, Y. Zhang, S. Ramakrishna and C. Lim, *Polymer,* 2004, **45**, 5361-5368.

20 S.Y. Gu, Z.M. Wang, J. Ren and C.Y. Zang, *Mater Sci Eng C,* 2009, **29**, 1822-1828.

21 M.E. Elsabee and E.S. Abdou, *Mater Sci Eng C.* 2013, **33**, 1819-1841.

22 J. Javad, H.E. Shahriar, S. Ali, A.B. Mohammad and G. Fazel, *Bio-Med Mater Eng,* 2011, **21**, 99-112.

23 H. Hu, H. Jiang, H. Ren, X. Hu, X. Wang and C. Han, *Diabetes Metabolism Res Rev,* 2014, DOI: 10.1002/dmrr.2560.

24 J. Chen, X. Chen, X. Yang, C. Han, C. Gao and Z. Gou, *Carbohyd Polym,* 2013, **92**, 612-20.

25 R. Augustine, E. A. Dominic, I. Reju, B. Kaimal, N. Kalarikkalac and S. Thomas, *RSC Advances*, 2014, **4**, 24777-24785.

26 S. Barua, G. Das, L. Aidew, A. K. Buragohain and N. Karak. *RSC Advances*, 2013, **3**, 14997-15004.

27 R.M. Nzietchueng, B. Dousset, P. Franck, M. Benderdour, P. Nabet and K. Hess, *J Trace Elem Med Biol,* 2002, **16**, 239-44.

28 X. Yang, L. Zhang, X. Chen, X. Sun, G. Yang, X. Guo, H. Yang, C. Gao and Z. Gou, *J Non-Crystal Solids,* 2012, **358**, 1171-1179.

29 J. Ye, X. Shi, X. Chen, J. Xie, C. Wang, K. Yao, C. Gao and Z. Gou, *J Mater Chem B,* 2014, **2**, 4226-4235.

30. T. Liu, D. Lai, Y. Chen, R. Zhang, X. Chen, X. Feng, X. Chen, X. Yang, R. Zhao, K. Chen, X. Kong, *J Mater Chem B*, 2014, **2**, 6293-6305.

31 C.N. Soparkar, J.F. Wong, J.R. Patrinely, J.K. Davidson and D. Appling, *Ophthalm Plastic Reconstruce Surg.,* 2000, **16**, 330-336.

32 W. Friess and G. Lee, *Biomaterials,* 1996, **17**, 2289-2294.

33 P. Sepulveda, J.R. Jones and L.L. Hench, *J Biomed Mater Res,* 2002, **61**, 301-311.

34 M.H. Fathi and M.A. Doost, *Mater Sci Eng A,* 2008, **474**, 128-33.

35 P.B. Van Wachem, A.H. Hogt, T. Beugeling, J. Feijen, A. Bantjes, J.P. Detmers and W.G. Van Aken, *Biomaterials,* 1987, **8**, 323-328.
36 P. Kunal, A.K. Banthia and D.K. Majumdar, *J Mater Sci: Mater Med,* 2007, **18**, 1889-1894.
37 C. Guo, L, Feng, J. Zhai, G. Wang, Y. Song and L. Jiang. *Chem Phys Chem*, 2004, **5**, 750-755.
38 F. Xia, L. Feng, S. Wang, T. Sun, W. Song, W. Jiang and L. Jiang. *Adv Mater*, 2006, **18**, 432-436.
39 D. Zhang, O Lepparanta, E. Munukka, H. Ylanen, K.V. Viljanen, E. Eerpla, M. Hupa, L. Hupa. *J Biomed Mater Res,* 2010, **93A**, 475-483.
40 F. Ding, H. Deng, Y. Du, X. Shi and Q. Wang. *Nanoscale*, 2014, **6**, 9477-9493.
41 R. ben-Knaz, R. Pedahzurb and D. Avnir. *RSC Advances*, 2013, **3**, 8009-8013.
42 I. Chopra, *J Antimicrobial Chemother-apy,* 2009, **59**, 587-590.
43 D.J. Leaper, *Int Wound J,* 2006, **3**, 282-294.
44 R.L. Gillette, S.F. Swaim, E.A. Sartin, D.M. Bradley and S.L. Coolman, *Am J Veterinary Res,* 2001, **62**, 1149-1156.
45 A.A. Gorustovich, C. Perio, J.A. Roether and A.R. Boccaccini, *Tissue Eng B:Review,* 2010, **16**, 199-210.
46 Z.P. Xie, C.Q. Zhang, C.Q. Yi, J.J. Qiu, J.Q. Wang and J. Zhou, *J Biomed Mater Res, Part B: Appl Biomater,* 2009, **90B**, 195-201.
47 P. Su, C. Wang, X. Yang, X. Chen, C. Gao, X.X. Feng, J.Y. Chen, J. Ye and Z. Gou, *Carbohydate Polym,* 2011, **84**, 239-246.

Graphics

Bioactive glass-introduced gelatin/chitosan nanofibrous dressings were developed via electrospinning to endow improved antibacterial activity, adjustable bioactivity and water uptake capacity for the requirement in enhancing chronic wound healing.